Non-Reciprocal Cavity Polariton with Atoms Strongly Coupled to Optical Cavity

Pengfei Yang, Ming Li, Xing Han, Hai He, Gang Li,* Chang-Ling Zou,* Pengfei Zhang, Yuhua Qian, and Tiancai Zhang*

Breaking the time-reversal symmetry of light is of great importance for fundamental physics and has attracted increasing interest in the study of non-reciprocal photonic devices. Here, a chiral cavity quantum electrodynamics system with multiple atoms strongly coupled to a Fabry–Pérot cavity is experimentally demonstrated. By polarizing the internal quantum state of the atoms, the time-reversal symmetry of the atom-cavity interaction is broken. The strongly coupled atom-cavity system can be described by non-reciprocal quasiparticles, that is, the cavity polariton. When it works in the linear regime, the inherent nonreciprocity makes the system work as a single-photon-level optical isolator. Benefiting from the collective enhancement of multiple atoms, an isolation ratio exceeding 30 dB on the single-quanta level (≈ 0.1 photon on average) is achieved. The validity of the non-reciprocal device under zero magnetic field and the reconfigurability of the isolation direction are also experimentally demonstrated. Moreover, when the cavity polariton works in the nonlinear regime, the quantum interference between polaritons with weak anharmonicity induces non-reciprocal nonclassical statistics of cavity transmission from coherent probe light.

P. Yang, X. Han, H. He, G. Li, C.-L. Zou, P. Zhang, T. Zhang
State Key Laboratory of Quantum Optics and Quantum Optics Devices, and Institute of Opto-Electronics
Shanxi University
Taiyuan 030006, China
E-mail: gangli@sxu.edu.cn; clzou321@ustc.edu.cn; tczhang@sxu.edu.cn
P. Yang, X. Han, H. He, G. Li, P. Zhang, T. Zhang
Collaborative Innovation Center of Extreme Optics
Shanxi University
Taiyuan 030006, China
M. Li, C.-L. Zou
CAS Key Laboratory of Quantum Information
University of Science and Technology of China
Hefei, Anhui 230026, P. R. China
Y. Qian
Key Laboratory of Computational Intelligence and Chinese Information Processing of Ministry of Education
Shanxi University
Taiyuan 030006, China

The ORCID identification number(s) for the author(s) of this article can be found under https://doi.org/10.1002/lpor.202200574

1. Introduction

Magnet-free optical non-reciprocal devices, in which the light propagates non-reciprocally from opposite directions, have great application potential in photonic information processing.[1,2] They also allow the realization of artificial gauge fields for photons and the simulation of interesting effects that were previously only available for electrons.[3,4] The optical nonreciprocity (ONR) intrinsically relies on the time-reversal (T) symmetry breaking of photon propagation, which was traditionally realized via a notable magneto-optical effect with the precondition of an intense external bias DC-magnetic field.[5] However, the strong magnetic field and the associated non-reconfigurable and non-switchable functionality greatly limits the applications.[6] Therefore, many efforts have been devoted to magnet-free ONR, including spatiotemporal modulation of dielectric permittivity,[7–11] synthetic magnetic field,[12–14] optics frequency conversion processes,[15–22] optomechanics,[23–28] chiral light–matter interaction,[29–31] the Doppler effect,[32–35] and light-induced magnetization[36] in atomic media, coherent interference of spin-waves,[37] spinning resonators,[38] etc. One of the most adopted approaches is to utilize coherent nonlinear optical effects, by which the direction-dependent transmission of the probe light is realized with a coherent external drive in a fixed direction[15–22] or a refractive index modulation with an effective momentum (p).[7–11] The T-symmetry is broken as $\mathcal{T} p \mathcal{T}^{-1} = -p$ with $\mathcal{T}$ being the time-reversal operator. All-optical nonreciprocity with such a mechanism has been experimentally verified in optomechanics and nonlinear microresonator platforms,[17,22,23,39] in which strong bias AC-driving fields are needed.

Alternatively, since $\mathcal{T} S \mathcal{T}^{-1} = -S$ for the spin operator S, the T-symmetry is naturally broken by preparing the internal spin state of atoms or emitters with $S \neq -S$. Therefore, when the photon interacts with atoms, assisted by the selection rules, the non-reciprocal transmission of the photon propagating along the z-direction could be realized by preparing the atoms to a ground state with biased spin state S_z. Recently, the strong coupling between single atoms or single quantum dots and chiral photons has been studied experimentally in a whispering-gallery-mode

(WGM) microresonator[40] and nanowaveguide,[41] where the non-reciprocal transmission of light fields can be realized via the unequal interaction strength between the emitters and photons with different chirality. The isolation[30] and circulation[42] of single photons have been demonstrated. In these experiments, the intrinsic chiral property of the evanescent field of the WGM microresonator or the nanowaveguide is adopted, but the achievable isolation ratio is limited to 13 dB due to the small atom number.

In this paper, the chiral light–matter interaction, where the interaction between atoms and two circular photons with orthogonal polarization are different, is introduced into the conventional cavity quantum electrodynamics (QED) with an optical Fabry–Pérot cavity (FPC) experimentally. The collective interaction between multiple atoms with a miniature high-finesse optical FPC greatly boosts the cooperativity of the system, and the strongly coupled photons and atoms constitutes the hybrid quasiparticles, which are called "cavity polaritons." The non-reciprocal polariton is then realized by preparing the atoms in a spin-polarized internal state with total spin $S \neq 0$, which asymmetrically couple to the two orthogonal circularly polarized cavity modes. The polariton inherently breaks the T-reversal symmetry and gives rise to non-reciprocal vacuum Rabi splitting spectra. By introducing polarizers and waveplates outside the cavity, the circular polarization of inputs to the cavity is locked with the direction of the inputs, and thus, the non-reciprocal polaritons enable an optical isolator with an isolation over 30 dB and a bandwidth exceeding 10 MHz. Compared to our previous demonstration of ONR by using few-atom nonlinear bistability,[43] which works on the few-photon level, this work is based on a vacuum-induced quantum process and works on the single-quanta level ($\approx$ **0.1** intracavity photon number on average). The isolation can be further enhanced by increasing the number of atoms. The direction of the isolation is reconfigurable by switching the internal state of spin-polarized atoms. The device is capable of working under a zero magnetic field with the aid of a circularly polarized optical pumping field propagating along the cavity to maintain the polarization of the atom.

Additionally, by employing the weak anharmonicity of the polaritons, nonclassical features of light can be generated non-reciprocally from coherent input light because of the quantum interference between polaritons. In particular, sub-Poissonian versus super-Poissonian photon statistics, or bunching versus antibunching effects, are observed when probing the system from different directions. Taking advantage of the few-atom cavity QED platform, the adjustable nonlinearity of non-reciprocal polaritons allows studies of potential non-reciprocal quantum effects and nonlinear dynamics. This new quasiparticle holds great potential for exploring quantum nonreciprocity in photonics[44,45] and quantum network applications,[46,47] chiral photophysics of molecules[48] and new topological effects of polaritons.[47,49–52]

2. Principle of Non-Reciprocal Cavity Polaritons

Figure 1 schematically illustrates the concept of the chiral atom-cavity system. A cavity QED setup with neutral atoms coupled to an FPC[43,53,54] is adopted. The cavity supports two degenerate circularly polarized optical modes (σ_+ and σ_-), which asymmetrically couple to the atoms. Here, the σ_+- and σ_--polarized fields are defined by the rotating direction of the electric field with respect to the direction of the quantization axis (z-axis). It is worth noting

that the $\sigma_\pm$ polarization is not related to the propagation direction of the photon. The $\sigma_\pm$-polarized field could be either a left-handed circularly polarized (LCP) field or a right-handed circularly polarized (RCP) field defined in optics, and the σ_+-polarized and σ_--polarized photons are chiral to each other (see Section S1, Supporting Information for details). In the following, we refer to the $\sigma_\pm$ notation for describing the chiral photon-atom interaction since the corresponding atomic transitions with respect to the quantization axis couple with the $\sigma_\pm$-polarized photon according to the selection rules.

As shown in Figure 1a,b, the σ_+-polarized light field couples to the atomic transition $|g\rangle \leftrightarrow |e\rangle$, whereas no atomic transition is available for the σ_--polarized light field. This situation can be easily found in an atom by preparing the atom to a ground spin-polarized state with Zeeman quantum number $m_F = -F$ (with the hyperfine quantum number $F \neq 0$) and using the atomic transition $|F\rangle \leftrightarrow |F'\rangle$ (with the hyperfine quantum number $F' \leq F$). The propagation direction of the signal light is not presented in Figure 1 because the interaction with the atom has no connection with the propagation direction. The collective atom-cavity coupling cooperativity for the σ_+-polarized mode is much greater than unity, and cavity polaritons between the photons and atoms are then constituted. The cavity polaritons, shown as quasiparticles with annihilation operator $p_{u,l} = \frac{1}{\sqrt{2}}(a_+ \pm b_+)$ at the low excitation limit (u and l denote the upper and lower polaritons respectively; see Section S5, Supporting Information for details), have eigenfrequencies detuned from the bare cavity by $\pm g_{\mathrm{eff}}$. Here, a_+ and b_+ denote the Bosonic operator of the σ_+-polarized cavity mode and the corresponding collective pseudospin operator for atomic transition, respectively, and g_{eff} is the effective coupling strength. Hence, the system shows two polariton states in the spectra (two peaks in Figure 1c), and both emit only σ_+-polarized photons. When the time is reversed, the σ_+-polarized photon becomes σ_-. The atoms are transparent to the σ_--polarized photons due to the absence of atomic transitions (Figure 1b). Thus, the mode remains as a bare cavity mode (Figure 1d). Comparing these two cases, it is obvious that the T-symmetry is broken for the atom-cavity interacting system.

The T-symmetry breaking of the system would break the Lorentz reciprocity of forward ($+z$) and backward ($-z$) propagating probe light with σ_+ and σ_- polarizations, respectively. Under the linear approximation (Section S4, Supporting Information), the transmission of the whole system reads

$$T_\pm = \frac{4\kappa_1\kappa_2}{\kappa^2} \left| \frac{1}{i\Delta/\kappa + 1 + 2C_\pm/(i(\Delta + \Delta_{\mathrm{ac}})/\gamma + 1)} \right|^2 \quad (1)$$

where $\pm$ indicates the probe light condition ($+z, \sigma_+$) or ($-z, \sigma_-$). Here, κ and $\kappa_{1(2)}$ denote the total decay rate of the cavity mode and the external coupling rate to the cavity through mirror M1 (M2), respectively. Δ (Δ_{ac}) is the frequency detuning of the cavity modes to probe laser (atomic transition), and $C_\pm = g_{\mathrm{eff},\pm}^2/(2\kappa\gamma)$ is the parameter of cooperativity for two σ-polarized cavity modes with $g_{\mathrm{eff},\pm} = g_\pm \sqrt{N_{\mathrm{eff}}}$, where N_{eff} is the effective intracavity atom number and $g_\pm$ is the coupling strength of the $\sigma_\pm$ cavity mode with one atom and depends on the atomic population distribution on the ground states. Beyond the linear approximation, the cavity polaritons actually exhibit anharmonicity for a finite atom
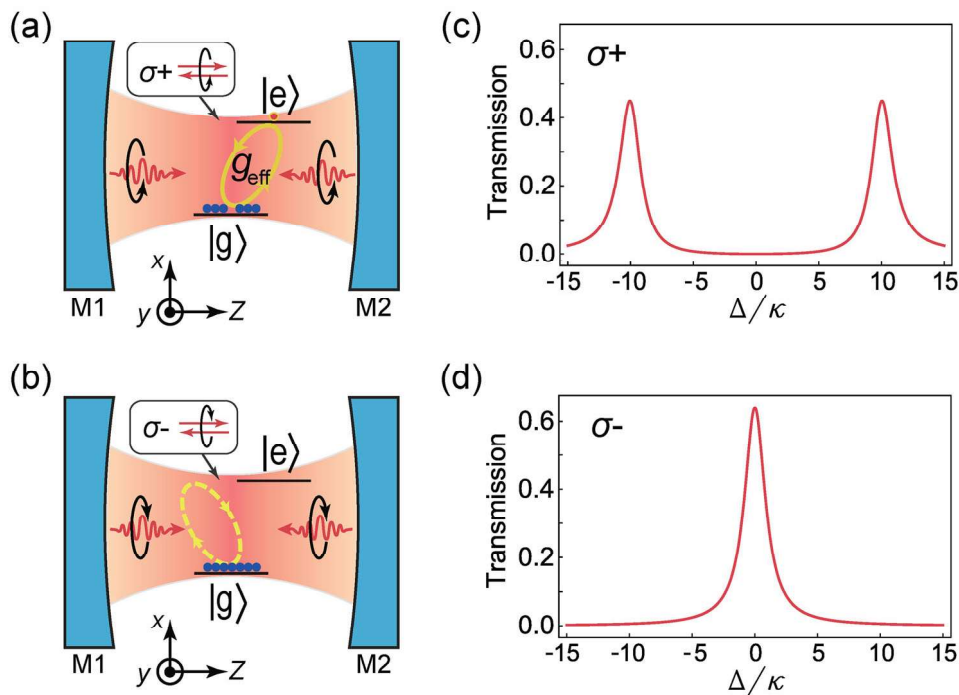
Figure 1. Chiral interaction between atoms and a Fabry–Pérot cavity. a,b) Schematic illustrations of the chiral interaction, in which the σ_+-mode of the cavity is strongly coupled to the atoms (a) but the σ_--mode is transparent (b) due to the absence of the atomic transition. Here, the σ_+-(σ_--) polarized field is defined by the rotating direction of the electric field with respect to the direction of the quantization axis (z-axis), which could be either an LCP field or an RCP field defined in optics (see Section S1, Supporting Information for details). In (a) and (b), ($+z$) is taken as the quantization axis along the cavity. The propagation direction of the light field is not presented because the interaction with the atom has no connection with the propagation direction. c,d) The theoretical predictions of the corresponding transmission spectra for the non-reciprocal interacting system by weak signals with polarizations of σ_+ (c) and σ_- (d), respectively. In (c), two polariton states (the hybrid atom-photon states) are obviously observed. The parameters of $C_+ = 50$, $C_- = 0$, $\kappa = \gamma_+ = 1$, and $g_{\text{eff}}/\kappa = 10$ are used for the calculation.

number, with an effective Kerr coefficient $\mp g_{\text{eff}}/2N_{\text{eff}}$ for $p_{u,l}$ (Section S5, Supporting Information). In general, the atoms in thermal equilibrium would give a uniform population on ground state Zeeman levels, and the spin polarization would be absent with $S = 0$. Both σ_+- and σ_--polarized light couple to atoms with the same strengths with $C_+ = C_-$; therefore, the system is reciprocal. For a polarized spin state with a slanted population distribution on Zeeman levels (nonuniform distribution with $S \neq 0$), Equation (1) predicts distinguishable spectra as $C_+ \neq C_-$, manifesting the non-reciprocity of the system.

3. Results

3.1. Experimental Setup

The experiments are performed on a cavity QED system with multiple cesium (Cs) atoms coupled to a miniature high-finesse FPC.[43] A sketch of the experimental system is shown in **Figure 2**a. A strongly coupled cavity QED system with multiple maximally spin-polarized Cs atoms is placed between the optical momentum-spin locking apparatuses, which consist of two sets of polarization beam splitters (PBSs) and quarter wave plates (QWPs), as shown in the dashed boxes of Figure 2a. The axis of the QWP is oriented 45° to the polarization of the transmitting light field from the PBS, and the optical axes of the two QWPs are orthogonal to each other. The probe light field with horizontally

linear polarization transmits the apparatuses in both directions (from a1 to b2 and from a2 to b1), and the polarization is locked to the propagating direction in the region between two QWPs, that is, the probe light can only be in either ($+z$, σ_+) or ($-z$, σ_-) states with a fixed quantization axis (green arrow). Without special declarations, a weak 3-Gauss magnetic field is used to define the quantization axis. Without the cavity QED system or if a cavity QED system with atomic spin $S = 0$ is considered, the optical system is reciprocal. However, the reciprocity will be broken if a non-reciprocal cavity QED system (with atomic spin $S \neq 0$) is placed between the two QWPs. The whole system resembles a commercial isolator except that the Faraday rotator is replaced by a non-reciprocal cavity QED system. It is worth noting that, like the Faraday-rotator-based optical isolator, this device can also be used as a four-port circulator, and here, we only use it as an isolator by neglecting the reflections from the two PBSs.

The FPC is assembled by two concave mirrors with curvature radii of 100 mm, and the cavity length is 335 μm. The concave surfaces are highly reflective, and the cavity has a finesse of 6.1×10^4. A 1064 nm optical dipole trap (ODT) laser beam (horizontal) with a waist of 36 μm is used to load cold atoms from the MOT and transfer the atoms to the cavity. To prepare atoms to the maximally spin-polarized internal state, $S_z = -4$ ($|6S_{1/2}, F = 4, m_F = -4\rangle$), a σ_--polarized 459 nm pump laser with a beam waist of 550 μm along the cavity axis and a linearly polarized 894 nm repump laser beam perpendicular to the cavity axis are used. The 459-
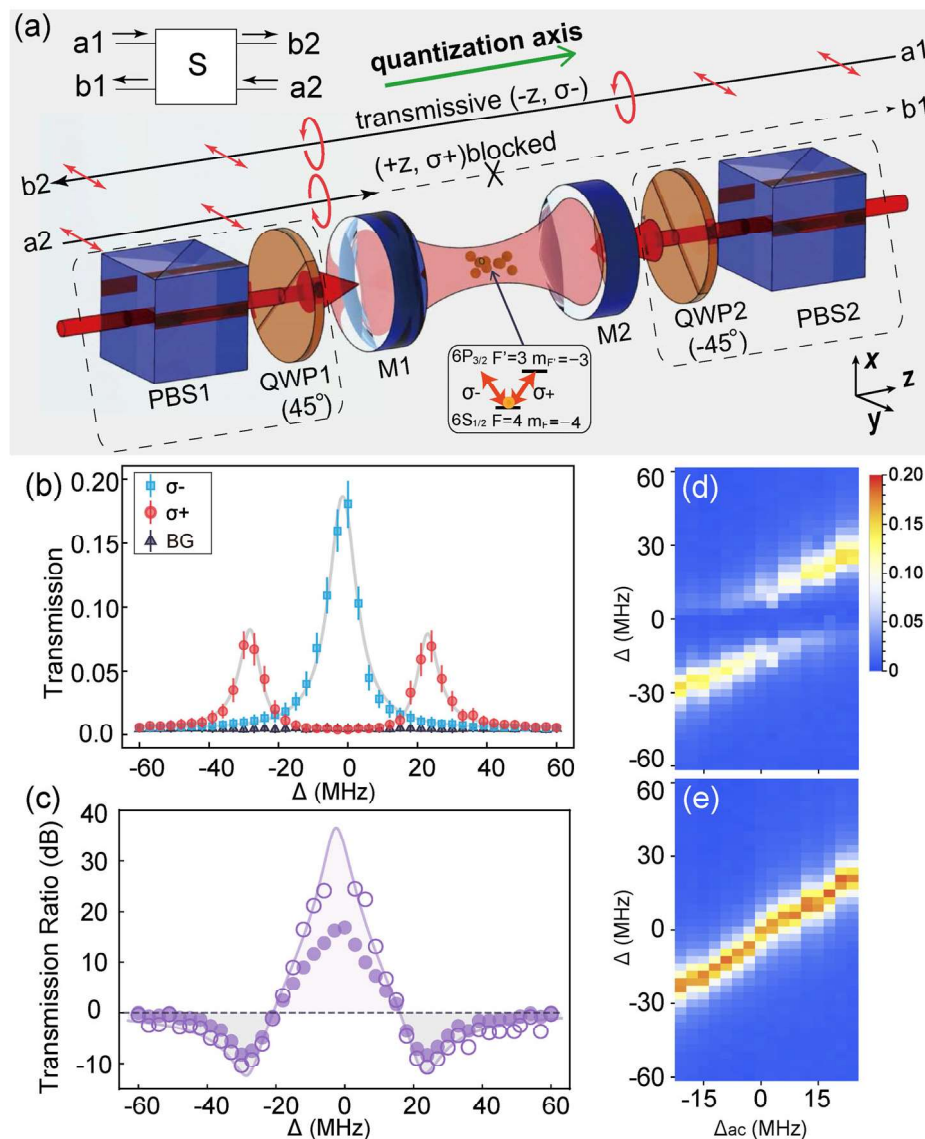
Figure 2. Experimental demonstration of the chiral cavity QED system and non-reciprocal polaritons. a) A sketch of the experimental setup. A strongly coupled cavity QED system between multiple maximally spin-polarized Cs atoms and the σ_+-polarized cavity mode is placed between two sets of PBSs and QWPs, where the locking of optical momentum-spin and the propagation direction can be realized. The quantization axis is along the cavity [green arrow, also the (+z) direction]. Red arrows indicate local optical polarization. A σ_+ polarized light propagating along the (+z) direction is blocked, while a σ_- polarized light propagating along the (−z) direction is transmitted. Insets: diagram of the atom energy levels (bottom) and scattering S matrix of the system (upper left corner). b) The measured transmission spectra with σ_+ (red circles) and σ_- (blue squares) polarized probes propagating along opposite directions. The background noise (black triangles) is shown as a comparison. The error bars correspond to one standard deviation of multiple measurements. The solid curves are the theoretical fittings by Equation (1). c) The measured transmission ratio between the $\sigma_\mp$-polarized probe versus detuning. The parameters are the same as in (b). The open and solid circles are the results with and without background correction, respectively, and the purple curve is the theoretical result. d,e) 2D spectra of the system probed by σ_+ (d) and σ_- (e) polarized light with the probe-cavity detuning Δ scanned at different cavity-atom detunings Δ_{ac}.

nm and 894-nm lasers are resonant to Cs transitions $|6S_{1/2}, F = 4\rangle \leftrightarrow |7P_{1/2}, F' = 4\rangle$ and $|6S_{1/2}, F = 3\rangle \leftrightarrow |6P_{1/2}, F' = 4\rangle$, respectively. The coupling strength between the σ_+-mode of the cavity and single atom is $g_+ = 2\pi \times 1.7$ MHz, and the decay rates of the cavity and the atom are $(\kappa, \gamma_+) = 2\pi \times (3.7, 2.6)$ MHz. When multiple atoms couple to the cavity, the collective coupling strength would surpass the decay rates of the cavity and atom and make the system work in the strong-coupling regime.

3.2. Demonstration of Non-Reciprocal Polaritons

To demonstrate the non-reciprocal polariton, the bare cavity mode is tuned to be resonant to the atomic transition $|6S_{1/2}, F = 4, m_F = -4\rangle \leftrightarrow |6P_{3/2}, F' = 3, m_{F'} = -3\rangle$. We thus realize the ideal model shown in Figure 1a,b as only the σ_+-mode couples to the atoms owing to the absence of an excited state for the σ_--transition ($C_- = 0$) (the energy levels can be found

**ADVANCED
SCIENCE NEWS**

www.advancedsciencenews.com

**LASER
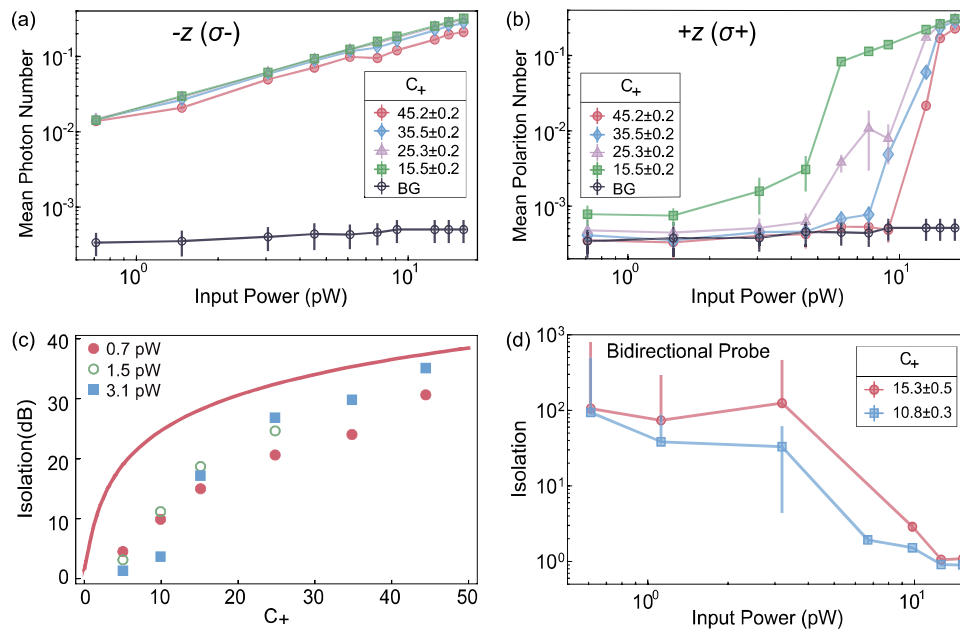&PHOTONICS
REVIEWS**

www.lpr-journal.org

Figure 3. Optical isolation based on the non-reciprocal cavity polaritons. a,b) The measured intracavity mean photon number under a series of cooperativity C_+ versus input power of the probe propagating along the $(-z)$ and $(+z)$ directions, respectively. c) The measured isolation versus cooperativity C_+ under a series of input powers. The red solid circles, green open circles, and blue solid squares are for input light with 0.7, 1.5, and 3.1 pW, respectively. d) The performance of the isolator with the forward and backward lights existing simultaneously, where the two lights have the same power. The corresponding cooperativities C_+ are 15.3(0.5) (red circles) and 10.8(0.3) (blue squares). The error bars correspond to one standard deviation.

in the inset of Figure 2a). The scattering matrix $(\mathbf{S_l})$ for the system is $\left(\begin{smallmatrix} 0 & 0 \\ \frac{4\kappa_1\kappa_2}{\kappa^2} & 0 \end{smallmatrix}\right)$ with $C_+ \gg 1$ and $\Delta = \Delta_{ac} = 0$ (see Section S4, Supporting Information for details).

By probing the system with $\sigma_\pm$-polarized light, we obtain the non-reciprocal vacuum Rabi splitting spectra, as shown in Figure 2b, which agree well with the theoretical predictions from Equation (1) (Figure 1c,d). Vacuum Rabi splitting is observed only from the σ_+-polarized probe, which indicates collective cooperativity $C_+ = 33.8(0.2)$ and an effective atom number $N_{eff} = 230.0(1.7)$. The atoms are optically pumped to the target spin state $|6S_{1/2}, F = 4, m_F = -4\rangle$ with a fidelity of $\approx 95\%$; thus, $C_- \ll C_+$ is still attained. The non-reciprocal polariton is further verified by the 2D spectra (Figure 2d,e), where the characteristic avoid-crossing spectra for polaritons can be accessed with only σ_+-polarized light as atom-cavity detuning Δ_{ac} being scanned.

In Figure 2b, if we focus on the frequency region around the atomic (or cavity) resonance, the transmission of the σ_+-polarized probe is blocked, but the σ_--polarized probe is transmitted. Since the two orthogonally polarized probe lights could only be injected into the cavity QED system from opposite directions, the whole system actually operates as an optical isolator. The isolation is defined by the transmission ratio $\mathcal{I} = T_-/T_+$. Figure 2c presents the measured $\mathcal{I}$ versus the probe detuning (Δ) with $\Delta_{ac} = 0$ and $C_+ = 33.8(0.2)$, showing both theoretical and experimental isolation over 20 dB with a bandwidth of 20 MHz. Around $\Delta \approx 0$, an isolation over 36.7 dB is expected from the theory, as the purple curve shows. However, the background-corrected experimental data points around $\Delta = 0$ are absent because the residual transmission of the blocked field is much weaker than the background,

which makes the background-corrected value inaccessible from the fluctuation of the background with the current data integration time of 100 μs. We believe the actual isolation around $\Delta = 0$ should be comparable with the theoretical prediction. We can also see that an isolation of approximately -10 dB can also be obtained when the probe is resonant to the polariton states.

The large $\mathcal{I}$ around zero detuning confirms the high performance of the optical isolator based on the non-reciprocal polariton in our scheme. From Equation (1), when $\Delta_{ac} = \Delta = 0$, the ideal isolation

$$\mathcal{I}_{max} = (1 + 2C_+)^2 \qquad (2)$$

would be achieved. $\mathcal{I}_{max}$ increases quadratically with the cooperativity C_+, and over 30-dB isolation can be achieved as $C_+ \geq 15.3$.

We then comprehensively investigate the performance of the isolator by varying the intracavity atom number (N_{eff}) and probe intensity under the condition $\Delta_{ac} = \Delta = 0$, and the results are summarized in **Figure 3**. The $(-z, \sigma_-)$ light couples to an empty cavity mode (Figure 1d), and the transmission depends linearly on the input light power (Figure 3a). The slight decrease in the transmission at larger C_+ is because of the scattering of the atom with imperfections in state preparations. An overall transmission of 18% is obtained and is limited by the impedance mismatch of the FPC.[43] A much higher transmission would be achieved by optimizing impedance matching of the cavity. For a given C_+, in Figure 3b, the transmission of the $(+z, \sigma_+)$ light is blocked at weak input power with a corresponding mean photon number less than 0.1, as expected. However, the input field can also excite the polariton modes off-resonantly, which would degrade

the isolation ratio as the input power increases with a fixed atom number. The polariton modes will be fully saturated at a certain input power which depends on the atom number. The larger C_+ (also the larger atom number) is, the more difficult it is for the polariton modes to be excited and the better the isolation obtained. The dependence of the measured isolation $\mathcal{I}$ on C_+ compared with the theoretical curve [Equation (2)] is shown in Figure 3c. Although the measured $\mathcal{I}$ is slightly lower than the theoretical value $\mathcal{I}_{max}$ (red solid curve), which is mainly limited by the experimental imperfections, such as background noise and the finite fidelity of the target spin-polarized atomic state preparation as discussed above, the measured isolation can still reach 30 dB with C_+ of ≈ 35.

3.3. Performance of the Optical Isolator with Two Opposite Laser Beams Coexisting

Different from many other magnet-free optical nonlinear nonreciprocal devices, the optical isolator demonstrated in this article can work in the condition with coexisting forward and backward light due to the decoupling of the two circularly polarized cavity modes. This property would dramatically expand the application. The isolation is experimentally verified with the input power varying in this bidirectional-probing scenario, and the data for $C_+ = 15.3(0.5)$ and $10.8(0.3)$ are shown by red circles and blue squares in Figure 3d, respectively. The behavior is quite similar to that of single-direction probing, where a higher C_+ gives higher isolation with weak input power. However, because both the forward and backward lights are shined, it is very difficult to separate the transmission of the backward light from the residual reflection of the forward light, and the measured isolation is slightly lower. The actual isolation should be the same as the case with an individual probing light field.

3.4. Reconfigurability of the Optical Isolator

Moreover, our device is reconfigurable by controlling the internal state of spin-polarized atoms. This is done experimentally by manipulating the population of the atomic Zeeman states. To verify this, the circularity of the 459-nm laser is switched between σ_- and σ_+ polarization with a time period of 15 ms to switch the atomic population between states $S_z = -4$ ($|6S_{1/2}, F = 4, m_F = -4\rangle$) and $S_z = 4$ ($|6S_{1/2}, F = 4, m_F = +4\rangle$) back and forth. The blocking and transmitting directions are then reconfigured accordingly (**Figure 4**). Here, a constant 1.5-Gauss magnetic field is applied to maintain the spin polarization of atoms. We find that the shut-off time 43 ± 2 μs is much faster than the turn-on time 705 ± 19 μs. The difference between these two switching times is due to the different joint effects of optical pumping and atom-cavity coupling in the two processes. The detailed analysis can be found in Section S11, Supporting Information. The theoretical curves of the switching calculated by taking both the optical pumping process and the atom-cavity couplings in all Zeeman states into account are also shown in Figure 4 (solid curves). The experimental results (open circles) are in good agreement with the theoretical prediction.
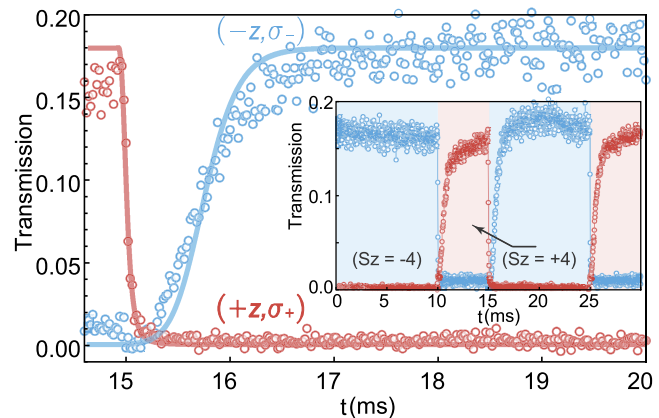

Figure 4. Reconfiguration of the isolation direction. Measured transmission as a function of time accompanied by atomic state switching between $S_z = -4$ and $+4$, where $C_{+(-)} = 20.5$. The blue open circles (experiment) and solid line (theory) are for forward light ($-z, \sigma_-$), and the red ones are for backward light ($+z, \sigma_+$). The switching times are 705 ± 19 and 43 ± 2 μs for the shut-off and turn-on processes, respectively. The inset shows the switching of the isolator continuously. The experimental data points are the average of 230 trials with 0.01 mean probe photons inside the FPC.

3.5. Validity of the Isolation without a Magnetic Field

The non-reciprocal cavity polariton and the demonstration of the aforementioned optical isolator are performed with a weak bias magnetic field. Notably, even such a weak magnetic field is not necessary for our current device. The performance of the isolation under a zero magnetic field is demonstrated and measured when the atoms are continuously pumped with a σ_--polarized 459 nm optical pumping laser, by which the spin direction of atoms can be preserved. The data are shown in **Figure 5**. Here, the atomic polarization is degraded due to the absence of the quantization axis previously defined by the magnetic field. However, the presence of the σ_--polarized 459 nm pump laser can weakly maintain the polarization, and thus, the system still gives non-reciprocal spectra, as shown in Figure 5a, where blue (red) open circles are for the σ_- (σ_+) polarized probe. The corresponding isolation of the probe light fields is shown in Figure 5b, which gives an isolation around 4 dB with a bandwidth over 30 MHz. It should be noted that by increasing the power of the polarized 459 nm optical pumping laser, a better isolation performance can be achieved.

3.6. Non-Reciprocal Quantum Statistics

The non-reciprocal polariton is then studied in more general cases since the maximally polarized spin state might not always be available in experiments. For example, as schematically illustrated in **Figure 6**a, both the σ_+- and σ_--modes of the cavity could strongly couple to the atomic transition with unequal strengths ($C_\pm \gg 0$ and $C_- \neq C_+$). The situation is realized by preparing the atom to state $|6S_{1/2}, F = 4\rangle$ with a slanted population on the Zeeman sublevels from $m_F = -4$ to $m_F = 4$ (yellow solid circles). The cavity is then tuned to be resonant to $|6S_{1/2}, F = 4\rangle \leftrightarrow |6P_{3/2}, F' = 5\rangle$. Owing to the unequal transition strength (arrows
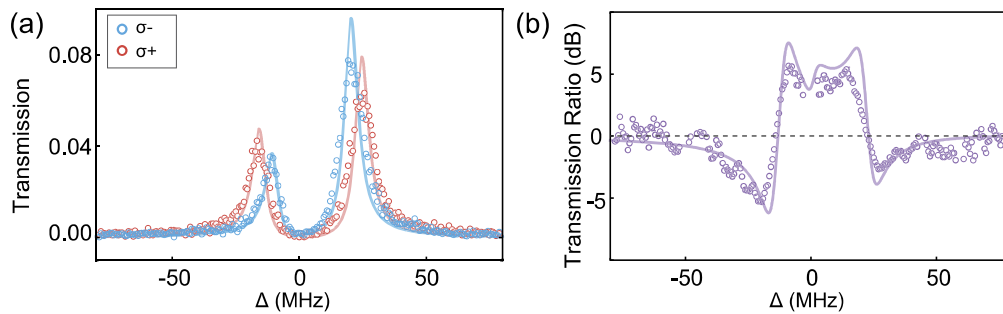
Figure 5. Validity of the isolation without a magnetic field. a) The non-reciprocal spectra for the σ_+ (open red circles) and σ_- (open blue circles) probes. The solid curves are the theoretical fittings by Equation (1). b) The transmission ratio with zero magnetic field, where a 4-dB isolation with bandwidth of 30 MHz is maintained. The purple solid curve is the theoretical expectation from the two fitting curves in (a).

with different thicknesses in Figure 6a), not only is the frequency of the polaritons asymmetric, but the strength of the nonlinearity experienced by the polariton is also different. The spectra of the polariton probed by weak coherent light, shown in Figure 6b, verify the nonreciprocity of the polariton. Here, the system is probed with σ_+- and σ_--polarized light both in the $(+z)$ direction, which is equivalent to the case in which the system is probed by the $(+z, \sigma_+)$- and $(-z, \sigma_-)$-probing configurations. The spectra of two σ_+-polaritons are asymmetric due to the off-resonant coupling between the bare cavity modes and other hyperfine energy levels ($|6P_{3/2}, F' = 4\rangle$) of the atoms, which induces a 6-MHz frequency shift in the effective cavity mode. In particular, such a dispersive effect is also non-reciprocal and is similar to the avoid-crossing results for large atom-cavity detuning in Figure 2d.

In such a few-atom cavity QED system, the anharmonicity of the polariton is inversely proportional to $\sqrt{N_{\text{eff}}}$ (Section S5, Supporting Information). The quantum effects of the polariton are greatly suppressed because the Kerr coefficient is much smaller than the system dissipation rate ($g_{\text{eff}}/2N_{\text{eff}} \ll \kappa, \gamma$). Surprisingly, we theoretically predict that the transmitted light exhibits remarkable quantum statistics for a classical input, as shown by the second-order correlation $g^{(2)}(0)$ in Figure 6b (blue and red dashed lines). When the probe is near resonant to the polariton states, the emissions of both $\sigma_\pm$-polaritons show a slight deviation from the Poissonian statistic ($g^{(2)}(0) = 1$) due to the weak anharmonicity of the polaritons. In contrast, much more pronounced non-reciprocity of the quantum statistics occurs around $\Delta = 0$, where the super-Poissonian distribution ($g^{(2)}_{\sigma_+}(0) > 1$) versus the sub-Poissonian distribution ($g^{(2)}_{\sigma_-}(0) < 1$) is expected (indicated by the vertical black-dotted line with mark "c" in Figure 6b). The physical mechanism behind the extraordinary behavior with $\Delta \approx 0$ is the quantum interference between the two polariton states $p_\pm$, which possesses a Kerr coefficient with opposite signs (Section S5, Supporting Information).

The experimental results of the temporal second-order correlation functions $g^{(2)}(\tau)$ for the $\sigma_\pm$-modes at $\Delta = 0$ are shown in Figure 6c, where the red (blue) cross markers are for the σ_+- (σ_--) mode. Here, we investigate the nonclassical statistics of the emission from cavity polaritons excited by a forwarding probe beam with fixed power. For the σ_+-polariton, the probe frequency is actually closer to one polariton state and shows a super-Poissonian distribution ($g^{(2)}(0) \approx 1.5$) and bunching ef-

fect ($g^{(2)}(0) > g^{(2)}(\tau)$). In contrast, the probe is equally off-resonant to both σ_--polaritons, where significant destructive interference of cavity polaritons takes place. The sub-Poissonian distribution ($g^{(2)}(0) \approx 0.8$) and anti-bunching effect ($g^{(2)}(0) < g^{(2)}(\tau)$) are displayed (Section S6, Supporting Information). The deviation between the experimental and theoretical results may be attributed to the noise background and system parameter uncertainties. Additionally, there are substantial oscillations in the temporal correlation function for both $\sigma_\pm$-polaritons, which indicate quantum interference between different polariton states. These results suggest that the anharmonicity of polaritons would bring non-reciprocal quantum features, which would extend the concept of non-reciprocal devices to the quantum regime[45] and provide experimental insights into the unconventional Bosonic blockade effect.[55]

4. Conclusion

Our demonstration of non-reciprocal polaritons from both linear and nonlinear aspects opens up a new perspective for research on cavity QED as well as novel non-reciprocal devices for photonics. The collective effect of a small atom ensemble produces polariton states as a hybridization of light and matter. By manipulating the atom at a maximally polarized state, the polariton can only be accessed optically from a certain direction, allowing isolation of photons with an isolation ratio exceeding 30 dB on the single-photon level. The reconfigurability of the isolation directions is experimentally demonstrated by switching the polarization of the atoms. The validity of the isolator with zero magnetic field is verified with relatively low isolation. By manipulating the quantum interference between the polaritons, the weak anharmonicity could still generate non-reciprocal nonclassical outputs from classical input. With the direction-dependent bunching and anti-bunching properties of polaritons being observed for the first time, our experiments show the potential for realizing both linear and nonlinear non-reciprocal optics effects on the single-quanta level. Such quantum non-reciprocal polariton states can be extended to phonons[56] and microwave photons[57,58] by harnessing their coupling with electron spin ensembles, and could find applications as quantum routers and isolators for quantum networks.[47] Our work also initiates the exploration of the concept of quantum nonreciprocity with
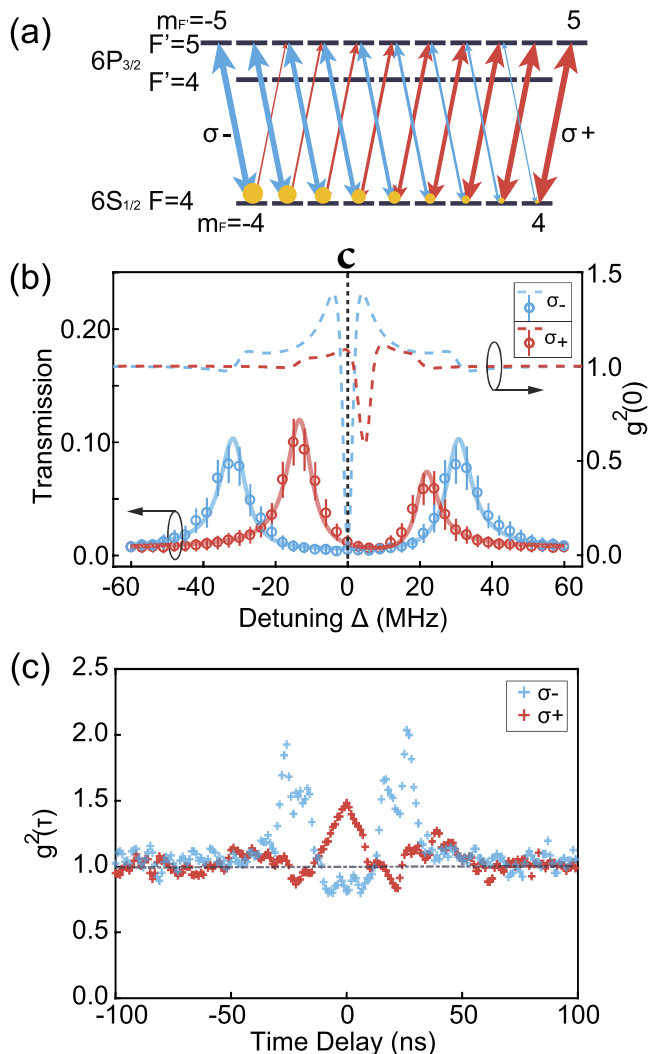
ADVANCED
SCIENCE NEWS _____

www.advancedsciencenews.com

LASER
& PHOTONICS
REVIEWS

www.lpr-journal.org

Figure 6. Quantum interference of polaritons and the nonreciprocity of quantum statistics. a) The energy diagram for realizing non-reciprocal polaritons under more general conditions. The atom ground spin state has a slanted population distribution on m_F. The size of yellow solid circles indicates the population in every Zeeman sublevel. The thickness of the blue (σ_-) and red (σ_+) arrows represents the corresponding σ-transition strength. b) The measured spectra by probing the system with σ_+ (red open circles) and σ_- (blue open circles) polarization. The fitting of the data gives $C_+ = 15.1(0.3)$, $C_- = 50.8(0.6)$, and $\Delta_{ac} = 0$ for the σ_- mode and $\Delta_{ac} = 6$ MHz for the σ_+ mode. The theoretical expectations of the second-order correlation function $g^{(2)}(0)$ are displayed as dashed curves, and the nonreciprocity of quantum statistics is clearly presented. c) The measured temporal second-order correlation function $g^{(2)}(\tau)$ by detecting the emitted photons from the cavity with the probe-cavity detuning fixed at 0 MHz. The error bars correspond to one standard deviation.

conventional quantum optics systems from two perspectives: on the one hand, polaritons are inherently a hybrid quantum state of photons and atoms, so superpositions of reciprocal and non-reciprocal polariton states are worth further investigation. On the other hand, we can study the quantum behaviors of non-reciprocal polaritons utilizing their intrinsic anharmonicity.

Supporting Information

Supporting Information is available from the Wiley Online Library or from the author.

Conflict of Interest

The authors declare no competing interests.

Data Availability Statement

The data that support the findings of this study are available from the corresponding author upon reasonable request.

[1] D. Jalas, A. Petrov, M. Eich, W. Freude, S. Fan, Z. Yu, R. Baets, M. Popović, A. Melloni, J. D. Joannopoulos, M. Vanwolleghem, C. R. Doerr, H. Renner, *Nat. Photonics* **2013**, *7*, 579.

[2] V. S. Asadchy, M. S. Mirmoosa, A. Díaz-Rubio, S. Fan, S. A. Tretyakov, *Proc. IEEE* **2020**, *108*, 1684.

[3] N. Goldman, G. Juzeliunas, P. Öhberg, I. B. Spielman, *Rep. Prog. Phys.* **2014**, *77*, 126401.

[4] D. Hey, E. Li, *R. Soc. Open Sci.* **2018**, *5*, 172447.

[5] R. J. Potton, *Rep. Prog. Phys.* **2004**, *67*, 717.

[6] L. Bi, J. Hu, P. Jiang, D. H. Kim, G. F. Dionne, L. C. Kimerling, C. a. Ross, *Nat. Photonics* **2011**, *5*, 758.

[7] Z. Yu, S. Fan, *Nat. Photonics* **2009**, *3*, 91.

[8] D.-W. Wang, H.-T. Zhou, M.-J. Guo, J.-X. Zhang, J. Evers, S.-Y. Zhu, *Phys. Rev. Lett.* **2013**, *110*, 093901.

[9] S. A. R. Horsley, J.-H. Wu, M. Artoni, G. C. La Rocca, *Phys. Rev. Lett.* **2013**, *110*, 223602.

[10] D. L. Sounas, A. Alù, *Nat. Photonics* **2017**, *11*, 774.

[11] H. Ramezani, P. K. Jha, Y. Wang, X. Zhang, *Phys. Rev. Lett.* **2018**, *120*, 043901.

[12] L. Tzuang, K. Fang, P. Nussenzveig, S. Fan, M. Lipson, *Nat. Photonics* **2014**, *8*, 701.

[13] L. Yuan, S. Xu, S. Fan, *Opt. Lett.* **2015**, *40*, 5140.

[14] K. Fang, J. Luo, A. Metelmann, M. H. Matheny, F. Marquardt, A. A. Clerk, O. Painter, *Nat. Phys.* **2017**, *13*, 465.

[15] A. Kamal, J. Clarke, M. Devoret, *Nat. Phys.* **2010**, *7*, 311.

[16] N. A. Estep, D. Sounas, J. Soric, A. Alù, *Nat. Phys.* **2014**, *10*, 923.

[17] S. Hua, J. Wen, X. Jiang, Q. Hua, L. Jiang, M. Xiao, *Nat. Commun.* **2016**, *7*, 13657.

[18] F. Song, Z. Wang, E. Li, Z. Huang, B. Yu, B. Shi, *Appl. Phys. Lett.* **2021**, *119*, 024101.

[19] C. Li, Q. Yu, Y. Zhang, M. Xiao, Z. Zhang, *Laser Photonics Rev.* **2023**, *17*, 2200267.

[20] L. Chang, X. Jiang, S. Hua, C. Yang, J. Wen, L. Jiang, G. Li, G. Wang, M. Xiao, *Nat. Photonics* **2014**, *8*, 524.

[21] K. Xia, F. Nori, M. Xiao, *Phys. Rev. Lett.* **2018**, *121*, 203602.

[22] X. Guo, C.-L. Zou, H. Jung, H. X. Tang, *Phys. Rev. Lett.* **2016**, *117*, 123902.

[23] Z. Shen, Y.-L. Zhang, Y. Chen, C.-L. Zou, Y.-F. Xiao, X.-B. Zou, F.-W. Sun, G.-C. Guo, C.-H. Dong, *Nat. Photonics* **2016**, *10*, 657.

[24] F. Ruesink, M.-A. Miri, A. Alù, E. Verhagen, *Nat. Commun.* **2016**, *7*, 13662.

[25] E. Verhagen, A. Alù, *Nat. Phys.* **2017**, *13*, 922.

[26] J. Kim, M. Kuzyk, K. Han, H. Wang, G. Bahl, *Nat. Phys.* **2015**, *11*, 275.

[27] M. Kang, A. Butsch, P. Russell, *Nat. Photonics* **2011**, *5*, 549.

[28] E. A. Kittlaus, W. M. Jones, P. T. Rakich, N. T. Otterstrom, R. E. Muller, M. Rais-Zadeh, *Nat. Photonics* **2021**, *15*, 43.

[29] I. Shomroni, S. Rosenblum, Y. Lovsky, O. Bechler, G. Guendelman, B. Dayan, *Science* **2014**, *345*, 903.

[30] I. Söllner, S. Mahmoodian, S. Lindskov Hansen, L. Midolo, A. Javadi, G. Kirsanske, T. Pregnolato, H. El-Ella, E. Hye Lee, J. Dong Song, S. Stobbe, P. Lodahl, *Nat. Nanotechnol.* **2015**, *10*, 775.

[31] O. Bechler, A. Borne, S. Rosenblum, G. Guendelman, O. Ezrah Mor, M. Netser, T. Ohana, Z. Aqua, N. Drucker, R. Finkelstein, Y. Lovsky, R. Bruch, D. Gurovich, E. Shafir, B. Dayan, *Nat. Phys.* **2018**, *14*, 996.

[32] S. Zhang, Y. Hu, G. Lin, Y. Niu, K. Xia, J. Gong, S. Gong, *Nat. Photonics* **2018**, *12*, 744.

[33] G. Lin, S. Zhang, Y. Hu, Y. Niu, J. Gong, S. Gong, *Phys. Rev. Lett.* **2019**, *123*, 033902.

[34] C. Liang, B. Liu, A.-N. Xu, X. Wen, C. Lu, K. Xia, M. K. Tey, Y.-C. Liu, L. You, *Phys. Rev. Lett.* **2020**, *125*, 123901.

[35] M.-X. Dong, K.-Y. Xia, W.-H. Zhang, Y.-C. Yu, Y.-H. Ye, E.-Z. Li, L. Zeng, D.-S. Ding, B.-S. Shi, G.-C. Guo, F. Nori, *Sci. Adv.* **2021**, *7*, eabe8924.

[36] X.-X. Hu, Z.-B. Wang, P. Zhang, G.-J. Chen, Y.-L. Zhang, G. Li, X.-B. Zou, T. Zhang, H. X. Tang, C.-H. Dong, G.-C. Guo, C.-L. Zou, *Nat. Commun.* **2021**, *12*, 2389.

[37] X. Lu, W. Cao, W. Yi, H. Shen, Y. Xiao, *Phys. Rev. Lett.* **2021**, *126*, 223603.

[38] S. Maayani, R. Dahan, Y. Kligerman, E. Moses, A. U. Hassan, H. Jing, F. Nori, D. N. Christodoulides, T. Carmon, *Nature* **2018**, *558*, 569.

[39] D. B. Sohn, S. Kim, G. Bahl, *Nat. Photonics* **2018**, *12*, 91.

[40] C. Junge, D. O'Shea, J. Volz, A. Rauschenbeutel, *Phys. Rev. Lett.* **2013**, *110*, 213604.

[41] C. Sayrin, C. Junge, R. Mitsch, B. Albrecht, D. O'Shea, P. Schneeweiss, J. Volz, A. Rauschenbeutel, *Phys. Rev. X* **2015**, *5*, 041036.

[42] M. Scheucher, A. Hilico, E. Will, J. Volz, A. Rauschenbeutel, *Science* **2016**, *354*, 1577.

[43] P. Yang, X. Xia, H. He, S. Li, X. Han, P. Zhang, G. Li, P. Zhang, J. Xu, Y. Yang, T. Zhang, *Phys. Rev. Lett.* **2019**, *123*, 233604.

[44] K. Xia, G. Lu, G. Lin, Y. Cheng, Y. Niu, S. Gong, J. Twamley, *Phys. Rev. A* **2014**, *90*, 043802.

[45] R. Huang, A. Miranowicz, J.-Q. Liao, F. Nori, H. Jing, *Phys. Rev. Lett.* **2018**, *121*, 153601.

[46] J. Borregaard, A. S. Sørensen, P. Lodahl, *Adv. Quantum Technol.* **2019**, *2*, 1800091.

[47] P. Lodahl, S. Mahmoodian, S. Stobbe, P. Schneeweiss, J. Volz, A. Rauschenbeutel, H. Pichler, P. Zoller, *Nature* **2017**, *541*, 473.

[48] S. Sun, B. Gu, S. Mukamel, *Chem. Sci.* **2022**, *13*, 1037.

[49] A. A. Houck, H. E. Türeci, J. Koch, *Nat. Phys.* **2012**, *8*, 292.

[50] *Quantum Simulations with Photons and Polaritons, Quantum Science and Technology*, (Ed: D. G. Angelakis), Springer, Cham **2017**.

[51] H. Zhao, X. Qiao, T. Wu, B. Midya, S. Longhi, L. Feng, *Science* **2019**, *365*, 1163.

[52] T. P. Lyons, D. J. Gillard, C. Leblanc, J. Puebla, D. D. Solnyshkov, L. Klompmaker, I. A. Akimov, C. Louca, P. Muduli, A. Genco, M. Bayer, Y. Otani, G. Malpuech, A. I. Tartakovskii, *Nat. Photonics* **2022**, *365*, 1163.

[53] J. M. Raimond, M. Brune, S. Haroche, *Rev. Mod. Phys.* **2001**, *73*, 565.

[54] A. Reiserer, G. Rempe, *Rev. Mod. Phys.* **2015**, *87*, 1379.

[55] H. J. Snijders, J. A. Frey, J. Norman, H. Flayac, V. Savona, A. C. Gossard, J. E. Bowers, M. P. Van Exter, D. Bouwmeester, W. Löffler, *Phys. Rev. Lett.* **2018**, *121*, 43601.

[56] D. A. Golter, T. Oo, M. Amezcua, K. A. Stewart, H. Wang, *Phys. Rev. Lett.* **2016**, *116*, 143602.

[57] S. Putz, D. O. Krimer, R. Amsüss, A. Valookaran, T. Nöbauer, J. Schmiedmayer, S. Rotter, J. Majer, *Nat. Phys.* **2014**, *10*, 720.

[58] A. Bienfait, J. J. Pla, Y. Kubo, X. Zhou, M. Stern, C. C. Lo, C. D. Weis, T. Schenkel, D. Vion, D. Esteve, J. J. L. Morton, P. Bertet, *Nature* **2016**, *531*, 74.